Investigating the usage of point spread functions in point source and microsphere localization

Jerry Chao[a,b], Sripad Ram[c], E. Sally Ward[b,d], and Raimund J. Ober[a,b]

[a]Dept. of Biomedical Engineering, Texas A&M University, College Station, TX 77843, USA
[b]Dept. of Molecular and Cellular Medicine, Texas A&M Health Science Center, College Station, TX 77843, USA
[c]Dept. of Electrical Engineering, University of Texas at Dallas, Richardson, TX 75080, USA
[d]Dept. of Microbial Pathogenesis and Immunology, Texas A&M Health Science Center, College Station, TX 77843, USA

ABSTRACT

Using a point spread function (PSF) to localize a point-like object, such as a fluorescent molecule or microsphere, represents a common task in single molecule microscopy image data analysis. The localization may differ in purpose depending on the application or experiment, but a unifying theme is the importance of being able to closely recover the true location of the point-like object with high accuracy. We present two simulation studies, both relating to the performance of object localization via the maximum likelihood fitting of a PSF to the object's image. In the first study, we investigate the integration of the PSF over an image pixel, which represents a critical part of the localization algorithm. Specifically, we explore how the fineness of the integration affects how well a point source can be localized, and find the use of too coarse a step size to produce location estimates that are far from the true location, especially when the images are acquired at relatively low magnifications. We also propose a method for selecting an appropriate step size. In the second study, we investigate the suitability of the common practice of using a PSF to localize a microsphere, despite the mismatch between the microsphere's image and the fitted PSF. Using criteria based on the standard errors of the mean and variance, we find the method suitable for microspheres up to 1 μm and 100 nm in diameter, when the localization is performed, respectively, with and without the simultaneous estimation of the width of the PSF.

Keywords: Cramér-Rao lower bound, Fisher information, localization accuracy, maximum likelihood estimation, microsphere, pixel integration, point spread function, single molecule microscopy

1. INTRODUCTION

In single molecule fluorescence microscopy, the fitting of a point spread function (PSF) to the image of a point-like object is commonly used to extract information about the object. In particular, PSF fitting has been widely employed for the estimation of the locations of individual fluorescent protein or dye molecules, and of individual microspheres each made up of many simultaneously fluorescing dye molecules. In the former case, the obtained positional coordinates have been used, for example, to reconstruct fluorescently labeled subcellular structures with very high resolution.[1–3] In the latter case, the estimated positional coordinates of microspheres have been used, for example, to correct for sample drift[2, 4–6] and to register spatially misaligned images acquired by different cameras[4] or in different color channels.[6–9]

In both cases, the obtained location estimates have direct implications on the interpretation of the image data and the results of any associated analyses. It is therefore important that the PSF fitting algorithm performs well, in the sense that it is able to closely recover the true locations of the molecules or microspheres, and to do so with a high level of accuracy. In this paper, we report two independent simulation studies, both having to do with the performance of the maximum likelihood fitting of a PSF in estimating the location of a point-like object. We have chosen to investigate the maximum likelihood estimator in both studies, as it has been demonstrated to have favorable properties in the context of the localization of point-like objects.[10–12]

Send correspondence to R.J.O. E-mail: raimund.ober@tamu.edu

In the first study, we explore how the fineness with which the PSF is integrated over each image pixel affects the performance of a location estimator. This question arises from the fact that the image of a point-like object, such as a single molecule, is a pixelated version of the continuous PSF, and that the mean number of photons in each pixel that are detected from the object is given by the integral of the PSF over the pixel. Therefore, as an estimator searches for the object location that produces the best fit of the PSF to the pixelated image, it must repeatedly compute integrals over the pixels, of versions of the PSF corresponding to different location values, until it finds the best-fit location. In terms of implementation, some research groups have chosen to accurately compute the integral over each pixel,[2, 10, 11] while others have elected to use a simple but less accurate method of integration that samples the PSF at only a single point over each pixel.[13] Naturally, good estimator performance can be expected with accurate integration that finely samples the PSF over each pixel. However, fine integration is expensive from the computational standpoint, and in certain cases, a coarser integration may provide satisfactory performance at a faster speed.

In our investigation, we examine the impact of the fineness of PSF integration on the performance of the maximum likelihood location estimator. We consider the maximum likelihood fitting of the Airy PSF, which results from optical diffraction theory,[14] as well as the two-dimensional (2D) Gaussian PSF, which some groups[15–17] use to localize single molecules, to images simulated with those PSFs. For both PSFs, we look at four different data scenarios that differ in the levels of object signal and additive noise sources. For each data scenario, we also consider two different magnifications, which we expect to impose different requirements on the fineness of PSF integration, by virtue of the different pixelations that they produce of a given PSF. We conclude our first study by proposing a method for obtaining a guideline to help determine a minimal fineness of integration that should be used in order to ensure an acceptable level of performance by the maximum likelihood location estimator.

In our second study, we consider the localization of a fluorescent microsphere by the fitting of a PSF to its image, and assess the suitability of this common approach to microsphere localization by evaluating the performance of the estimator. Microsphere localization using, for example, the Airy PSF or the 2D Gaussian PSF, is predicated on the fact that a small microsphere is point-like, and hence produces an image that is similar to the microscope's PSF. It is therefore typical to find that microspheres no greater than 200 nm in diameter are used in applications such as drift correction[2, 4–6] and image registration.[4, 6–9] The use of such small microspheres in these applications is consistent with guidelines suggesting that a microscope's PSF is best approximated by the image of a microsphere whose diameter is substantially smaller than the microscope's theoretical resolution, such as given by the Rayleigh criterion.[18–20] Though microsphere localization by PSF fitting is commonly carried out, and despite the fact that small microspheres are reasonably point-like, there remains the question of whether, given the mismatch between the microsphere's image and the fitted PSF, the estimator is able to closely recover the microsphere's true location with a high level of accuracy.

We address the question of suitability by evaluating the performance of the maximum likelihood fitting of an Airy PSF to simulated microsphere images. We consider three scenarios that differ by the wavelength of the detected photons, and for each scenario, we assess the effect of microsphere size by applying the maximum likelihood location estimator to microspheres of diameters ranging from 50 nm to 1 μm. For every data set considered, we explore two approaches to the localization. In one approach, the width of the fitted Airy PSF is fixed at its theoretical value, and only the positional coordinates of the PSF are estimated. In the other approach, the width of the fitted Airy PSF is estimated along with the positional coordinates, thus allowing the maximum likelihood estimator to better match the PSF to the images of larger microspheres, and in doing so, enable it to better determine the positional coordinates of larger microspheres. Based on our results for each approach, we make an assessment as to the microsphere sizes that are suitable for localization by PSF fitting.

In our studies, the performance of the maximum likelihood location estimator is key to determining the appropriateness of a particular setting, be it the fineness of PSF integration or the size of a microsphere. This performance is quantified and evaluated in similar ways in the two studies. Given estimates of the location obtained from repeat images of a molecule or microsphere, the closeness with which the estimator recovers the true object location is quantified by the difference between the mean or median of the estimates and the true location. For the same estimates, the level of accuracy is quantified by the percentage difference between the standard deviation of the estimates and the best possible standard deviation, as determined using Fisher information theory,[21] that can be attained for the given image data. In the first study, the performance of an

estimator is deemed acceptable if both these quantities are comparable to the corresponding quantities for the benchmark estimator which uses the same fineness of PSF integration as was used to simulate the image data. In the second study, an estimator's performance is considered acceptable if both these quantities satisfy certain threshold criteria based on the standard errors of the mean and variance for an ideal estimator that recovers the microsphere's true location and attains the best possible standard deviation for the given image data.

Note that both the fineness of PSF integration study[22] and the microsphere localization study[23] have been recently reported elsewhere. Here, we give a condensed presentation of each study, and provide an entirely new set of results that supplement the previously reported results. Note that for the microsphere localization study, results of estimations carried out on experimental images of microspheres can be found in our previous report.[23]

2. THEORY AND METHODS COMMON TO BOTH STUDIES

The two studies presented in this paper have much in common in terms of mathematical foundation and methods. In the following subsections, we describe the image model, the method of image data simulation, the method of maximum likelihood location estimation, and the Fisher information-based measure for quantifying the level of an estimator's accuracy, all of which are applicable to both studies.

2.1 Image model

The emission of photons by a fluorescent molecule or microsphere is an intrinsically stochastic phenomenon. The detection of those photons is therefore also stochastic in nature, and is typically modeled as a Poisson process. Accordingly, in our image model, the number of photons detected in the kth image pixel from a stationary object of interest is represented by the Poisson random variable $S_{\theta,k}$ with mean $\mu_{\theta,k}$ given by

$$\mu_{\theta,k} = \frac{N_{photon}}{M^2} \int_{C_k} q\left(\frac{x}{M} - x_0, \frac{y}{M} - y_0\right) dx dy, \tag{1}$$

where q is the image function[24] which describes the image of the object, at unit lateral magnification, when the object is located at the origin of the object space coordinate system, C_k is the region in the detector plane occupied by the pixel, M is the lateral magnification of the microscope system, N_{photon} is the mean number of photons detected over the detector plane per acquisition interval (i.e., per image), and x_0 and y_0 are the positional coordinates of the object. The subscript θ in $\mu_{\theta,k}$ denotes the function's dependence on the vector $\theta \in \Theta$ of parameters to be estimated from the acquired image, Θ being the parameter space. In this paper, we are interested in estimating the positional coordinates of a molecule or microsphere, and we therefore have $\theta = (x_0, y_0)$, and Θ an open subset of $\mathbb{R}^2$.

For an in-focus molecule, the image function q according to optical diffraction theory is the Airy PSF

$$q(x,y) = \frac{J_1^2(\alpha\sqrt{x^2 + y^2})}{\pi(x^2 + y^2)}, \quad (x,y) \in \mathbb{R}^2, \tag{2}$$

where J_1 is the first order Bessel function of the first kind, and $\alpha = 2\pi n_a/\lambda$, where n_a is the numerical aperture of the objective lens and λ is the wavelength of the detected photons. We refer to α as the *width parameter*, as its value determines how broad the Airy PSF is. The smaller its value, the broader the Airy PSF. It is the additional parameter that is estimated in the microsphere localization approach that estimates the width of the fitted Airy PSF along with the positional coordinates x_0 and y_0 of the microsphere.

For the 2D Gaussian PSF model commonly used for an in-focus molecule, the image function is given by

$$q(x,y) = \frac{1}{2\pi\sigma_g^2} \cdot e^{-\frac{x^2+y^2}{2\sigma_g^2}}, \quad (x,y) \in \mathbb{R}^2, \tag{3}$$

where σ_g is the standard deviation of both the x and y component one-dimensional Gaussian functions.

For an in-focus microsphere modeled as a uniform distribution of fluorescent dye molecules throughout a spherical volume, the image function q is given by the convolution of the microscope's PSF and a ball centered at the origin of the object space coordinate system, and can be expressed as[23]

$$q(x,y) = \frac{3}{4\pi r^3} \int_0^{2\pi} \int_0^{\pi} \int_0^r PSF_{z_0} \left(x - \xi \sin\psi \cos\phi, y - \xi \sin\psi \sin\phi\right) \xi^2 \sin\psi \, d\xi \, d\psi \, d\phi, \quad (x,y) \in \mathbb{R}^2, \quad (4)$$

where r is the radius of the ball representing the microsphere, and PSF_{z_0} is the PSF observed at the detector plane for a point source located axially at the z coordinate $z_0 = \xi \cos\psi$ in object space. The PSF is dependent on the particular microscope, and for our study, we assume the classical PSF of Born and Wolf[14] given by

$$PSF_{z_0}(x,y) = \frac{4\pi n_a^2}{\lambda^2} \left| \int_0^1 J_0 \left(\frac{2\pi n_a}{\lambda} \sqrt{x^2 + y^2} \rho\right) e^{\frac{j\pi n_a^2 z_0}{n\lambda} \rho^2} \rho d\rho \right|^2, \quad (x,y) \in \mathbb{R}^2, \quad z_0 \in \mathbb{R}, \quad (5)$$

where J_0 is the zeroth order Bessel function of the first kind, n_a and λ are as defined above for the Airy PSF, and n is the refractive index of the objective lens immersion medium.

Besides photons from the object of interest, photons due to other sources, which we refer to collectively as the background component, are likewise detected according to a Poisson process. Hence, for the kth image pixel, we represent the number of detected background photons by the Poisson random variable B_k with mean β_k.

Furthermore, assuming that the image is acquired using a charge-coupled device (CCD) camera, the primary noise source due to the image detector itself is its readout electronics. Readout noise is typically assumed to be Gaussian-distributed, and accordingly, for the kth image pixel, we model the readout noise as a Gaussian random variable W_k with mean η_k and standard deviation σ_k.

In our image model, the data in the kth pixel of an image is thus the sum of the Poisson random variable $S_{\theta,k}$, the Poisson random variable B_k, and the Gaussian random variable W_k. The three random variables are mutually independent, since they result from three independent processes.

2.2 Image simulation

A CCD image of a fluorescent molecule or microsphere is simulated according to the image model of Section 2.1. A K-pixel image is generated as a sequence of pixel values $(z_1, z_2, \ldots, z_K)$, where for $k = 1, \ldots, K$, the value $z_k \in \mathbb{R}$ is the sum of two random numbers.

The first random number is a realization of the sum of the Poisson random variables $S_{\theta,k}$ and B_k, respectively representing the number of molecule or microsphere photons and the number of background photons that are detected in the kth pixel. It is drawn from the Poisson distribution with mean $\mu_{\theta,k} + \beta_0$, where β_0 is a nonnegative constant representing the mean of the background photon count in each pixel. The background photon count level is the same for all pixels (i.e., $\beta_k = \beta_0$ for $k = 1, \ldots, K$) as we assume a uniform background component over the entire image. Note that in calculating $\mu_{\theta,k}$ as given by Eq. (1), the region C_k over which the image function q is integrated is the square region corresponding to the kth pixel.

The second random number is a realization of the Gaussian random variable W_k representing the number of electrons in the kth pixel due to the readout process of the CCD camera. It is drawn from the Gaussian distribution with mean $\eta_0 \in \mathbb{R}$ and standard deviation $\sigma_0 > 0$. Note that we have the same readout noise distribution for all pixels (i.e., $\eta_k = \eta_0$ and $\sigma_k = \sigma_0$ for $k = 1, \ldots, K$) because in a CCD camera, all pixels are read out by the same readout electronics.

A simulated data set consists of 1000 repeat images of a molecule or microsphere, each generated, for $k = 1, \ldots, K$, with the same Poisson mean $\mu_{\theta,k} + \beta_0$ and the same Gaussian mean η_0 and standard deviation σ_0. In our implementation, the Poisson and Gaussian random numbers are respectively generated using MATLAB's *poissrnd* and *randn* functions.

Note that in the fineness of PSF integration study, data scenarios 1 and 3 correspond to data sets that are not corrupted by background and readout noise. For these data sets, the value z_k of the kth pixel, $k = 1, \ldots, K$, is simply a nonnegative integer drawn from the Poisson distribution with mean $\mu_{\theta,k}$.

2.3 Maximum likelihood localization

The maximum likelihood location estimator determines the positional coordinates $\theta = (x_0, y_0)$ of a molecule or microsphere from a given image by maximizing the log-likelihood function for the image with respect to θ. For a K-pixel image with pixel values $(z_1, z_2, \ldots, z_K)$, the log-likelihood function $\mathcal{L}(\theta \mid z_1, \ldots, z_K)$ is given by

$$\mathcal{L}(\theta \mid z_1, \ldots, z_K) = \sum_{k=1}^{K} \ln(p_{\theta,k}(z_k)), \tag{6}$$

where $p_{\theta,k}$ is the probability density or mass function of the data z_k in the kth pixel. For the CCD image model described in Section 2.1, the probability density function of the data z_k is the convolution of a Poisson probability mass function and a Gaussian probability density function, given by

$$p_{\theta,k}(z_k) = \frac{1}{\sqrt{2\pi}\sigma_k} \sum_{l=0}^{\infty} \frac{[\mu_{\theta,k} + \beta_k]^l e^{-(\mu_{\theta,k}+\beta_k)}}{l!} e^{-\frac{1}{2}\left(\frac{z_k-l-\eta_k}{\sigma_k}\right)^2}, \quad z_k \in \mathbb{R}. \tag{7}$$

For the Poisson image model of data scenarios 1 and 3 in the fineness of PSF integration study, the probability mass function of the data z_k is the Poisson probability mass function

$$p_{\theta,k}(z_k) = \frac{[\mu_{\theta,k}]^{z_k} e^{-\mu_{\theta,k}}}{z_k!}, \quad z_k = 0, 1, \ldots. \tag{8}$$

In our implementation, the negative of Eq. (6) is minimized using MATLAB's *fminunc* function.

Note that in the microsphere localization study, for the approach wherein the width of the fitted Airy PSF is estimated along with its positional coordinates, Eq. (6) is maximized with respect to $\theta = (x_0, y_0, \alpha)$.

2.4 Limit of the localization accuracy

As pointed out in Section 1, the level of accuracy of a maximum likelihood location estimator in both of our studies is quantified by the percentage difference between the standard deviation of the location estimates and the best possible standard deviation that is attainable for the given image data. This best possible standard deviation, which we refer to as the *limit of the localization accuracy*, is given by the square root of the Cramér-Rao lower bound[21] for the estimation of the location parameter.

In general, given the vector θ of parameters to be estimated from the image data, the Cramér-Rao lower bound is obtained by first calculating the Fisher information matrix $\mathbf{I}(\theta)$. For the CCD image model detailed in Section 2.1, the Fisher information matrix for a K-pixel image has been shown to be[10, 24]

$$\mathbf{I}(\theta) = \sum_{k=1}^{K} \left(\frac{\partial \mu_{\theta,k}}{\partial \theta}\right)^T \frac{\partial \mu_{\theta,k}}{\partial \theta} \cdot \left(\int_{\mathbb{R}} \frac{\left(\sum_{l=1}^{\infty} \frac{[\mu_{\theta,k}+\beta_k]^{l-1} e^{-(\mu_{\theta,k}+\beta_k)}}{(l-1)!} \cdot e^{-\left(\frac{z-l-\eta_k}{\sqrt{2}\cdot\sigma_k}\right)^2}\right)^2}{2\pi\sigma_k^2 \cdot p_{\theta,k}(z)} dz - 1\right), \tag{9}$$

where $p_{\theta,k}$ is the probability density function given by Eq. (7). For the Poisson image model where the data z_k in the kth pixel is characterized by the Poisson probability mass function of Eq. (8), the Fisher information matrix for a K-pixel image is given by[10, 24]

$$\mathbf{I}(\theta) = \sum_{k=1}^{K} \left(\frac{\partial \mu_{\theta,k}}{\partial \theta}\right)^T \frac{\partial \mu_{\theta,k}}{\partial \theta} \cdot \frac{1}{\mu_{\theta,k}}. \tag{10}$$

Once we have the Fisher information matrix, the Cramér-Rao lower bound corresponding to the jth parameter in θ is obtained as the jth main diagonal element of the inverse of the matrix, which we denote by $\left[\mathbf{I}^{-1}(\theta)\right]_{jj}$.

In our studies, the Fisher information matrix is computed with the parameter vector $\theta = (x_0, y_0)$. Since the lower bound is a bound on the variance of any unbiased estimator of the jth parameter, we have that the *limit of the x-localization accuracy* and the *limit of the y-localization accuracy* (i.e., the best possible standard deviations for estimating x_0 and y_0, respectively) are given by $\sqrt{[\mathbf{I}^{-1}(\theta)]_{11}}$ and $\sqrt{[\mathbf{I}^{-1}(\theta)]_{22}}$, respectively.

3. STUDY 1: FINENESS OF PSF INTEGRATION

The maximum likelihood estimator determines the positional coordinates $\theta = (x_0, y_0)$ of a molecule from a given image by maximizing the log-likelihood function of Eq. (6) with respect to θ. Whether Eq. (6) is evaluated with the CCD probability density function of Eq. (7) or the Poisson probability mass function of Eq. (8), the estimator ultimately has to compute the mean number of molecule photons detected in each image pixel by calculating $\mu_{\theta,k}$ of Eq. (1) for each pixel k. During the maximization, this computation is performed potentially many times as the estimator attempts different values of x_0 and y_0 until it finds the values that maximize Eq. (6). Since $\mu_{\theta,k}$ is given by the integral of the PSF, in the form of the image function q, over the kth pixel, its repeated computation with different values of x_0 and y_0 means that the maximum likelihood estimator must integrate the PSF potentially many times over each pixel k. A fine integration will incur a higher computational time for the overall estimation of x_0 and y_0, but should in principle not affect the performance of the estimator in a negative way. On the other hand, a coarse integration will improve the speed of the estimation, but may negatively impact the performance of the estimator as it produces a less accurate value for the integral. The objective of this study is to investigate the impact of the fineness of this PSF integration on the performance of the maximum likelihood localization of a molecule, and to propose a method for obtaining a guideline for determining a minimal fineness of integration that ensures an acceptable level of estimator performance.

3.1 Method of investigation

To study the impact of the fineness of PSF integration on the performance of the maximum likelihood location estimator, we carry out estimations that utilize integration of coarser levels of fineness than that which is used to generate the image data.

We specify the fineness of integration over a square pixel in terms of a number we refer to as the *pixel integration factor* (PIF). A PIF value of 0 specifies the simple integration method in which the integral in Eq. (1) is approximated by the product of the area of the pixel and the value of the image function q at the center of the pixel. As illustrated in Fig. 1(a), this amounts to the approximation of the volume under the PSF and over the pixel by the volume of the rectangular box having the pixel as its base and the value of the PSF at the center of the pixel as its height. Since this method of integration requires the evaluation of the PSF at only a single point per pixel, the PIF = 0 scenario is importantly representative of the type of integration adopted by some research groups.[13]

As exemplified by the illustrations of PIF = 1, 2, 3, and 4 in Fig. 1(b), a PIF value of n, where $n = 1, 2, \ldots$, specifies integration that samples the PSF at $(n+1)^2$ evenly spaced points that cover the area of the given pixel. Therefore, a larger value of n means a finer level of integration. In our study, we use the 2D trapezoidal method of numerical integration.

For our investigation, data sets consisting of 1000 repeat images of a single molecule were simulated as described in Section 2.2 using either the Airy PSF (Eq. (2)) or the 2D Gaussian PSF (Eq. (3)). Each data set was simulated using a PIF value of 13, and was subjected to fourteen rounds of maximum likelihood localization, each corresponding to the use of a different PIF value in the range of 0 to 13 for the integration of the PSF over the image pixels.

To incorporate into our study conditions that are representative of different experimental settings, the data sets were simulated under the four scenarios shown in Table 1, which differ in terms of the levels of signal (i.e., photons detected from the molecule) and additive noise (i.e., photons due to the background component and electrons due to the detector's readout process). Scenarios 1 and 2 specify high signal levels, while scenarios 3 and 4 specify relatively low signal levels. Furthermore, whereas scenarios 1 and 3 specify no additive noise and therefore represent very ideal conditions, scenarios 2 and 4 specify additive noise levels that are relatively low and high, respectively, with respect to their signal levels.

For each of the four scenarios, data sets were simulated with the two commonly used magnifications $M = 100$ and $M = 63$. The magnification is of particular interest because it affects how the image of a molecule is pixelated, and therefore can be expected to be a determinant of how finely the PSF needs to be integrated over the image pixels.
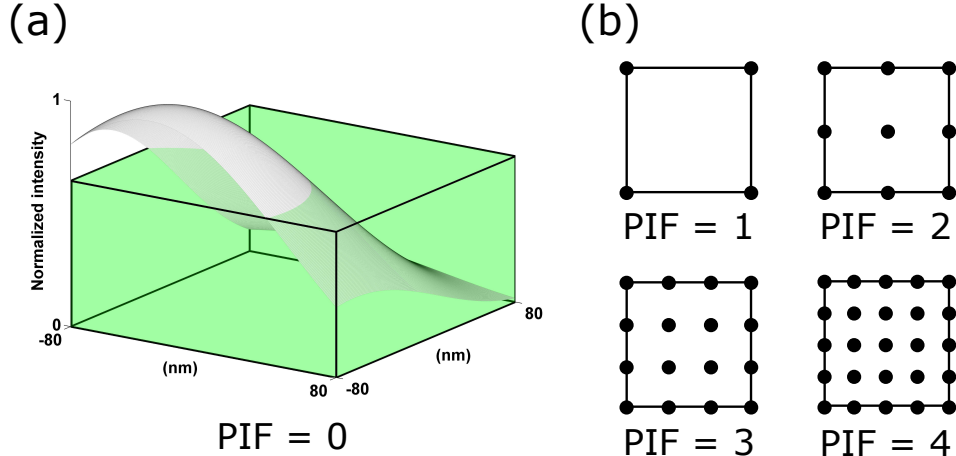
Figure 1. Fineness of PSF integration over a square pixel as specified by the pixel integration factor (PIF). (a) A PIF value of 0 specifies the simple integration method that approximates the mean number of molecule photons detected in a pixel as the rectangular volume (shown in green) given by the product of the area of the pixel and the value of the PSF (shown as a gray surface) at the center of the pixel. (b) A PIF value of n, where $n = 1, 2, \cdots$, specifies the computation of the integral of the PSF over a pixel, using a numerical integration method such as the 2D trapezoidal method employed in the current study, by evaluating the PSF at $(n + 1)^2$ evenly spaced sampling points that cover the area of the pixel.

For all data sets, the size of an image is 11×11 pixels, and the size of each pixel is 16 μm $\times$ 16 μm. The molecule is positioned such that its image (i.e., the PSF) is centered at 5.3 pixels in the x direction and 5.1 pixels in the y direction within the 11×11-pixel image. For $M = 100$ ($M = 63$), this equates to positional coordinates $\theta = (x_0, y_0) = (848 \text{ nm}, 816 \text{ nm})$ ($\theta = (x_0, y_0) = (1346.03 \text{ nm}, 1295.24 \text{ nm})$) for the single molecule, as the origin of the coordinate system is assumed to coincide with the upper left corner of the 11×11-pixel image. Also for all data sets, the numerical aperture of the objective lens is $n_a = 1.4$, and the wavelength of the detected photons is $\lambda = 485$ nm. Note that the wavelength is what differentiates the Airy PSF data sets here from the Airy PSF data sets analyzed in our previous report,[22] which were simulated with $\lambda = 669$ nm. The use of a smaller wavelength here means that we have a larger width parameter α for the Airy PSF (see Eq. (2)), and hence a narrower Airy PSF. Accordingly, we also use a smaller width of $\sigma_g = 72.94$ nm here for the 2D Gaussian PSF. In our previous report,[22] the 2D Gaussian PSF data sets were simulated with a width of $\sigma_g = 100.62$ nm.

3.2 Quantifying and evaluating estimator performance

For each data set, the performance of the maximum likelihood estimator is quantified in two respects. To quantify the estimator's ability to closely recover the true location of the molecule, we take the difference d between the median of the 1000 estimates of each positional coordinate and the true value of the coordinate. For the x_0 coordinate, for example, we have

$$d(x_0) = \text{median}(\hat{x}_0) - x_0, \tag{11}$$

where $\hat{x}_0$ denotes the maximum likelihood estimate of x_0, as represented by the 1000 estimated values. Note that instead of looking at the mean of the estimates, we choose to look at the more robust median of the estimates in order to prevent our analysis from being unduly influenced by outlying estimates. We have had evidence of outliers, for example, in the estimates for data sets corresponding to scenario 4, where the signal level is relatively low and the additive noise levels are relatively high.

To quantify the accuracy with which the estimator determines the location of the molecule, we calculate the percentage difference δ between the standard deviation (with respect to the median) of the 1000 estimates of each positional coordinate and the best possible standard deviation with which the coordinate can be estimated, as given by the limit of the localization accuracy presented in Section 2.4. Again using the x_0 coordinate as an example, the percentage difference, taken with respect to the limit of the x-localization accuracy, is given by

$$\delta(x_0) = \frac{\text{sd}(\hat{x}_0) - \lim(x_0)}{\lim(x_0)} \times 100, \tag{12}$$

Table 1. Signal and additive noise levels for the four data scenarios considered for the fineness of PSF integration study.

Scenario	Mean number N_{photon} of single molecule photons	Mean number β_0 of background photons per pixel	Mean η_0 of readout noise (e^-/pixel)	Std. dev. σ_0 of readout noise (e^-/pixel)
1	3000	0	0	0
2	3000	50	0	2
3	300	0	0	0
4	300	100	0	6

where sd denotes the standard deviation and lim denotes the limit of accuracy. The latter is calculated using the Fisher information expression of Eq. (9) for scenarios 2 and 4, and of Eq. (10) for scenarios 1 and 3, with the underlying image function given by either Eq. (2) or Eq. (3) depending on the data set in question, and with all the same parameters as for the simulation of the data set, including the PIF value of 13.

For a given PIF value used for localization, the performance of the maximum likelihood location estimator is considered acceptable if the resulting differences d and δ are comparable in magnitude to the differences d and δ obtained for the estimator that uses the PIF value of 13. The results obtained for the PIF $= 13$ estimator are used as the benchmark because PIF $= 13$ was used to simulate the image data.

3.3 Results and Discussion

For each of the four scenarios of Table 1, we show, in separate plots and as a function of the PIF value used by the maximum likelihood estimator, the difference d between the median of the location estimates and the true location, and the percentage difference δ between the standard deviation of the estimates and the limit of the localization accuracy. Only the results for the x_0 coordinate are shown, as the results for the y_0 coordinate are similar. Note that for each data set presented, we also analyzed an additional data set that was statistically identical, and found the results to agree well with the results shown here. The results for the Airy PSF data sets are presented in Fig. 2, and the results for the 2D Gaussian PSF data sets are presented in Fig. 3.

We begin by examining the results for the benchmark PIF value of 13. For all four scenarios and both the $100\times$ and $63\times$ magnifications, the plots of Figs. 2 and 3 show that the difference d is close to zero at PIF $=$ 13, indicating that the maximum likelihood estimator is capable of closely recovering the true value x_0. More specifically, for all four scenarios and both magnifications in Fig. 2, the magnitude of d at PIF $= 13$ is no greater than 0.96 nm (the magnitude of d at PIF $= 13$ for scenario 4, $100\times$ magnification). Similarly, for all four scenarios and both magnifications in Fig. 3, the magnitude of d at PIF $= 13$ is no greater than 0.99 nm (the magnitude of d at PIF $= 13$ for scenario 4, $63\times$ magnification).

In terms of the accuracy of the estimator, the magnitude of the percentage difference δ at PIF $= 13$, in both Figs. 2 and 3, is no greater than 6% (the magnitude of δ at PIF $= 13$ for scenario 1, $63\times$ magnification, in Fig. 3) for scenarios 1, 2, and 3, and for both magnifications. The small percentages suggest that when N_{photon}, the mean number of photons detected from the single molecule, is large in comparison to noise from both the background component and the camera's readout process, the accuracy of the maximum likelihood location estimator will be comparable to the limit of the localization accuracy. In contrast, in the case of scenario 4 where N_{photon} is not large in comparison to the extraneous noise, δ at PIF $= 13$ can be relatively big, indicating that the accuracy of the estimator may not be as close to the limit of accuracy under such conditions. In our examples this is particularly the case for the $63\times$ magnification, where the magnitude of δ at PIF $= 13$ is 41% for the Airy PSF data set, and 29% for the 2D Gaussian PSF data set.

We next consider the results for the simple integration method represented by PIF $= 0$. In terms of the ability of the estimator to recover the true value x_0, the plots of Figs. 2 and 3 show that this simple method can lead to a difference d that is substantially larger in magnitude (i.e., worse) than d at PIF $= 13$. For the $63\times$ magnification, for example, the magnitude of d at PIF $= 0$, in each of the four scenarios, is greater than 41 nm in Fig. 2, and greater than 7 nm in Fig. 3. These magnitudes are extremely large, when compared to the magnitudes of d at PIF $= 13$, which as pointed out above are under 1 nm in all cases.

Scenario 1

Scenario 2

Scenario 3

Scenario 4
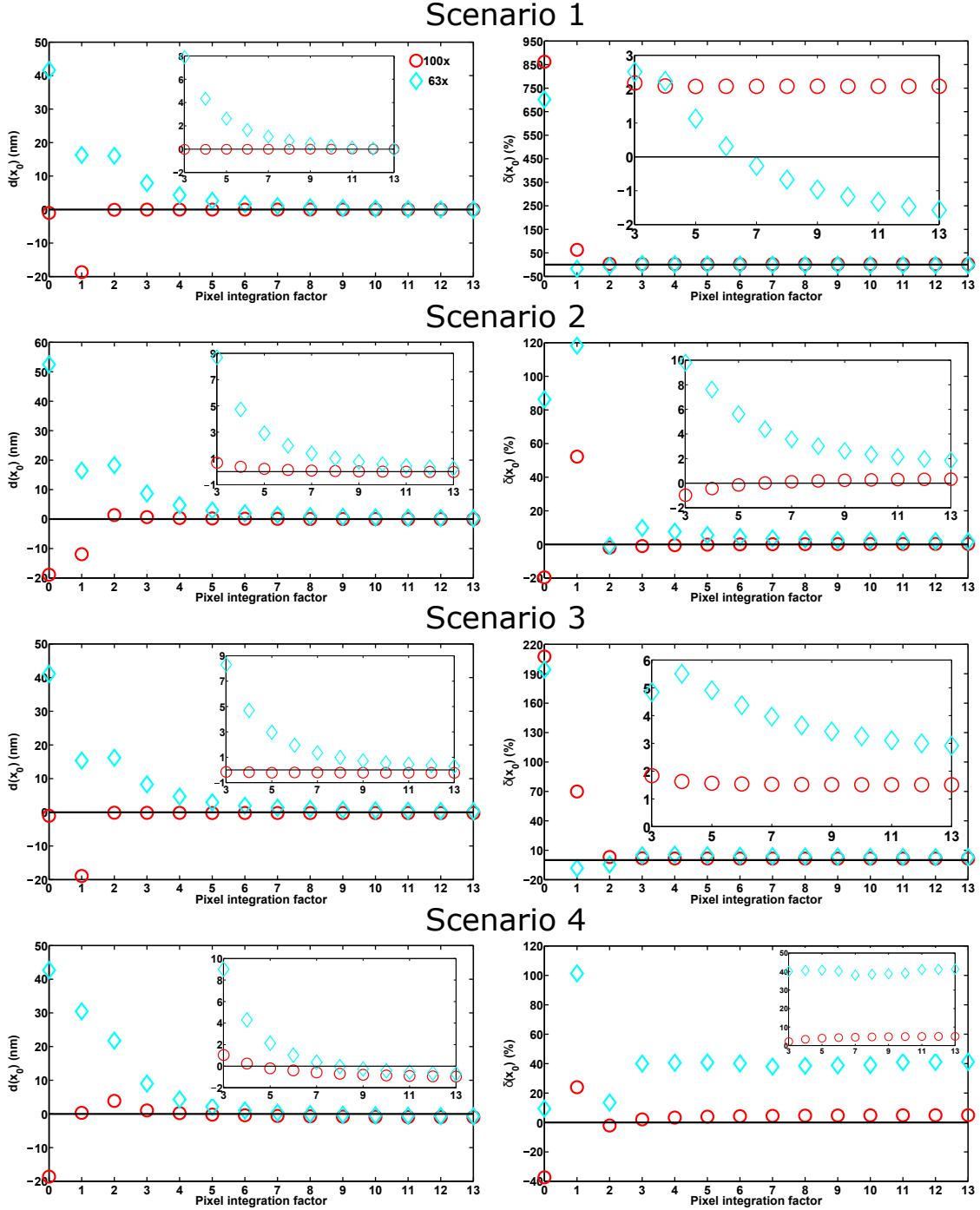
Figure 2. Airy PSF fineness of integration results: difference $d(x_0)$ between the median of the x_0 estimates and the true value x_0 (left-hand side plots), and percentage difference $\delta(x_0)$ between the standard deviation (with respect to the median) of the x_0 estimates and the limit of the x-localization accuracy (right-hand side plots), as functions of the PIF used to integrate the PSF during estimation. For each scenario of Table 1, results are shown for a 63× (cyan ⋄) and a 100× (red ∘) data set, simulated at PIF = 13 using the Airy PSF with the parameters given in Section 3.1. Each data set is fitted with an Airy PSF by a maximum likelihood estimator, with PIF values ranging from 0 to 13. In all plots the horizontal line denotes 0, and the inset shows the results for PIF ≥ 3.
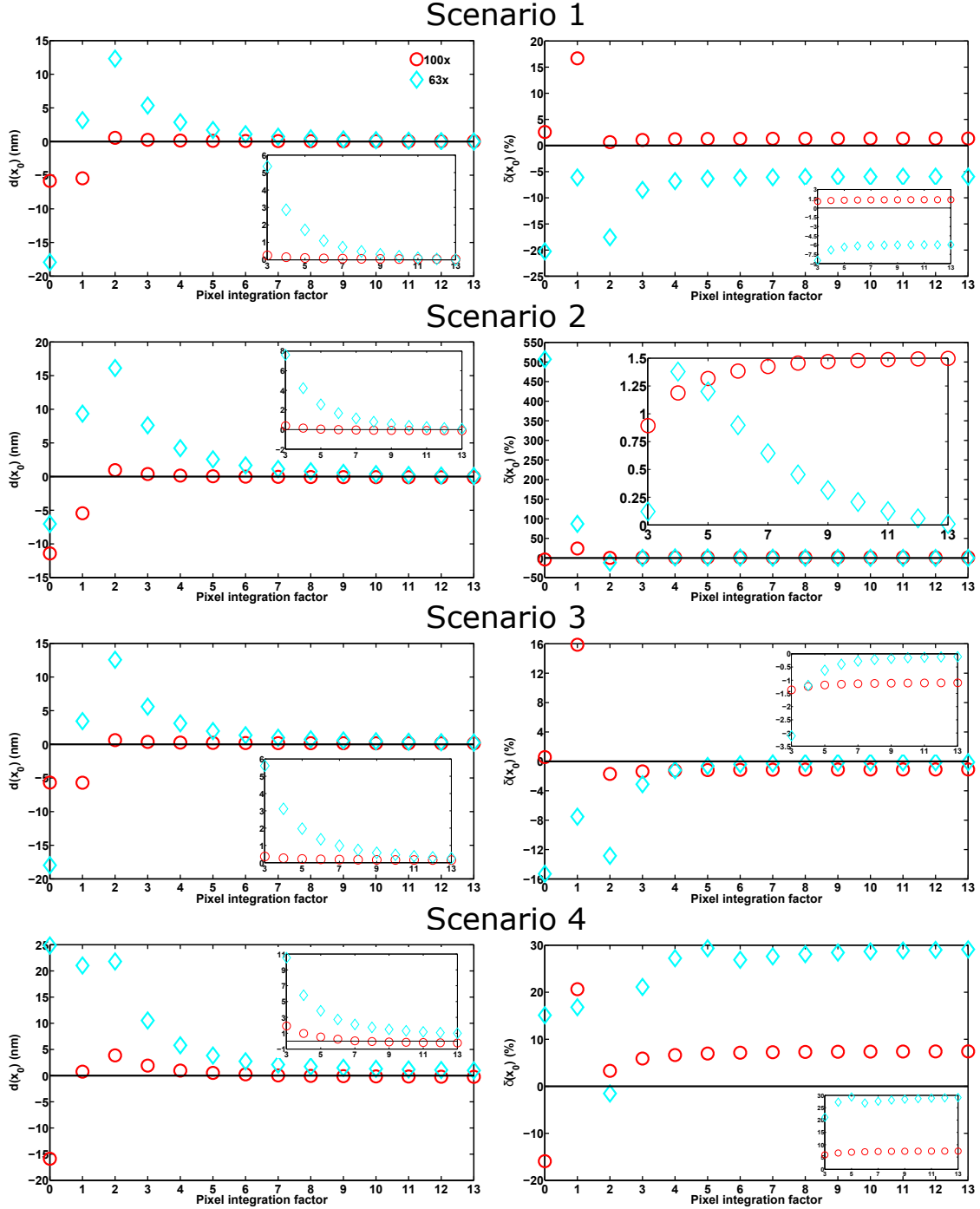
Figure 3. 2D Gaussian PSF fineness of integration results: difference $d(x_0)$ between the median of the x_0 estimates and the true value x_0 (left-hand side plots), and percentage difference $\delta(x_0)$ between the standard deviation (with respect to the median) of the x_0 estimates and the limit of the x-localization accuracy (right-hand side plots), as functions of the PIF used to integrate the PSF during estimation. For each scenario of Table 1, results are shown for a 63× (cyan $\diamond$) and a 100× (red $\circ$) data set, simulated at PIF = 13 using the 2D Gaussian PSF with the parameters given in Section 3.1. Each data set is fitted with a 2D Gaussian PSF by a maximum likelihood estimator, with PIF values ranging from 0 to 13. In all plots the horizontal line denotes 0, and the inset shows the results for PIF ≥ 3.

Except for scenarios 1 and 3 in Fig. 2, the magnitude of d at PIF $= 0$ is also very large for the $100\times$ magnification. Even for the two exceptions, however, the d magnitude of around 1 nm in each case is nontrivially larger than the corresponding d magnitude at PIF $= 13$, which is well below 1 nm. Moreover, even if the d magnitudes of around 1 nm were deemed acceptable, the δ values for these two cases are so much larger than the corresponding δ values at PIF $= 13$ that the performance of the estimator would still be considered very poor.

Though not seen with the data sets in the current study, the simple integration method represented by PIF $= 0$ can in fact yield d and δ values that are comparable in magnitude to d and δ obtained for PIF $= 13$. This was seen, for example, in our previous report[22] for the $100\times$ 2D Gaussian PSF data sets of scenarios 1, 2, and 3. The same is not observed for the corresponding data sets here, however, likely because of the significantly smaller width of $\sigma_g = 72.94$ nm for the 2D Gaussian PSF considered here. The larger width of $\sigma_g = 100.62$ nm in the previous study means that the shape of the 2D Gaussian PSF over each image pixel is flatter, so that for a given pixel, the rectangular volume given by the product of the area of the pixel and the value of the PSF at the center of the pixel makes a better approximation of the integral of the PSF over the pixel. An illustration of this is given in Fig. 4 using the Airy PSF. In the figure, one can see the shape of the PSF, over the pixel containing the PSF's peak, flatten as the PSF is broadened via a reduction of the numerical aperture from $n_a = 1.4$ to $n_a = 1.2$ to $n_a = 1.0$. Quantitatively, the percentage difference between the integral of the Airy PSF over the pixel and the approximating rectangular volume is correspondingly reduced from 26% to 21% to 16%.

Comparison of our results here with the results from our previous study therefore suggests that, by virtue of its ability to provide a better approximation of the integrals of the PSF over the image pixels in the case of a broader PSF, the simple integration method of PIF $= 0$ can sometimes lead to an estimator performance that is comparable to the performance of the benchmark estimator. To further demonstrate this, we analyzed additional $100\times$ 2D Gaussian PSF data sets, simulated according to scenarios 1 and 2, that differ by the width σ_g of the PSF. As expected, the results presented in Table 2 show that, for both scenarios, as the width of the 2D Gaussian PSF is increased from $\sigma_g = 72.94$ nm to $\sigma_g = 113.47$ nm, the d values as well as the δ values for the PIF $= 0$ estimator and the PIF $= 13$ estimator become more comparable. Note that these results are again corroborated by the results obtained for a second set of statistically identical data sets. Note also that since the idea is to have a flatter PSF shape over each image pixel, the PIF $= 0$ estimator can in principle also be expected to perform better if, instead of broadening the PSF (by, for example, decreasing the numerical aperture or increasing the wavelength of detection), we increase the magnification. The same effect can generally be expected, since a higher magnification yields smaller effective pixels that capture smaller, and hence flatter, portions of the PSF.

Lastly, we consider the results for estimation using PIF values ranging from 1 to 12, which represent coarser 2D trapezoidal integrations of the PSF than the benchmark PIF $= 13$ with which the image data was simulated. For all four scenarios and both the $100\times$ and $63\times$ magnifications, the plots of Figs. 2 and 3 show that the difference d converges to d at PIF $= 13$ as the PIF is increased from 1 to 12. This convergence points to the importance of integrating at a sufficiently fine step size. Our results suggest that this is particularly important when the images are acquired at a relatively low magnification. By looking at the insets for the d plots in both figures, one can see that for PIF $= 3$ and above, d as a function of the PIF at the $100\times$ magnification is essentially flat relative to d as a function of the PIF at the $63\times$ magnification, indicating that while one may be able to use small PIF values at higher magnifications, larger PIF values are needed at lower magnifications in order to obtain a d value that is comparable to that obtained using the benchmark PIF.

The plots of Figs. 2 and 3 also show the percentage difference δ to converge to δ at PIF $= 13$ when the PIF is increased from 1 to 12. Importantly, the same observation concerning the need to use larger PIF values at lower magnifications can be made by comparing the convergence of δ, as a function of the PIF, between the two magnifications.

The difference in the PIF's degree of impact between the two magnifications can be attributed to the fact that at higher magnifications, the pixels of the image capture smaller, and therefore flatter, portions of the PSF, thereby allowing the value of the integral over each pixel to be relatively well approximated by the use of a coarse integration. Small PIF values are therefore better suited, and can be utilized to improve the computational speed, for integration at higher magnifications.
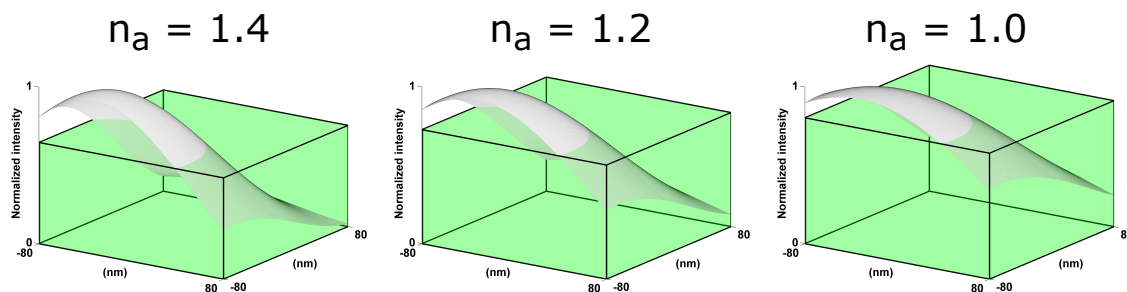
Figure 4. The Airy PSF over a pixel for three different values of the numerical aperture n_a. In each case, the Airy PSF is shown as a gray surface, and the rectangular volume used by the simple integration method of PIF $= 0$ to approximate its integral over the pixel is shown in green. The Airy PSF computed with $n_a = 1.4$ is the one used for the Airy PSF data sets analyzed in the current study, and the pixel shown is the center pixel of the 11×11-pixel image in the case of a $100\times$ magnification. The other two Airy PSFs are computed with the same parameters, but with n_a changed to 1.2 and 1.0. By reducing n_a from 1.4 to 1.2 to 1.0 (and hence broadening the PSF), the percentage difference between the integral of the PSF over the pixel and the rectangular volume is reduced from 26% to 21% to 16%.

The results of Figs. 2 and 3 clearly demonstrate the need to use a sufficiently fine PSF integration to ensure an acceptable performance by the maximum likelihood location estimator. There remains the question, however, of how one can determine the minimum PIF value that is needed. To address this question, we propose a method for obtaining a guideline that helps with the selection of an appropriate PIF.

We hypothesize that the differences in the performance of the maximum likelihood estimator at different PIF values are attributable to the differences between the PSFs computed using the different PIF values. Therefore, to arrive at a guideline for choosing an appropriate PIF, we quantify the difference between the PSF computed using a given PIF value and the PSF computed using the benchmark PIF value. Specifically, for a given position of the single molecule, we calculate a percentage difference by taking the absolute difference between the values of each pair of corresponding pixels in the two PSFs, and dividing the sum of all the absolute differences by the sum of the values of all pixels in the benchmark PSF. To take into account different positions of the molecule within the image, which yield different values for the pixels, we calculate the percentage differences for 121 positions of the molecule that cover one quadrant of the image's center pixel at regular spacings, and take the maximum of the 121 percentage differences to be the value that quantifies the difference between the benchmark PSF and the PSF for the given PIF value. We choose the maximum percentage difference because it represents the worst case, of all the positions considered, for the given PIF value. By looking at the worst case, the guideline that we obtain will be conservative, in the sense that it might specify a minimum PIF value that is higher than necessary. This is preferable, however, to the possibility of underestimating the minimum PIF value.

Note that with the current study in mind, the above method assumes the single molecule to be located within the center pixel of a square image consisting of an odd number of pixels. It also assumes that 121 regularly spaced positions of the molecule provide a reasonable sampling of a quadrant of the center pixel, which is all that needs to be sampled given the symmetry of the square image. Along with the selection of the maximum percentage difference, all of these specifications can be tailored as needed to produce a customized guideline for a given analysis setting.

For the Airy and 2D Gaussian PSFs considered in the current study, the maximum percentage difference was determined for PIF values of 0 to 13, and for both the $63\times$ and the $100\times$ magnifications. These maximum percentage differences are shown as a function of the PIF in Fig. 5, and they apply to all four scenarios of Table 1 as they do not depend on the level of the signal from the molecule or the levels of the additive noise sources.

From the figure we see that the curves corresponding to the four combinations of PSF and magnification are qualitatively similar, and as expected, they show that the PSF becomes more and more similar to the benchmark PSF (i.e., the maximum percentage difference decreases) as the PIF is increased. Compared with the $d(x_0)$ and $\delta(x_0)$ curves from the plots of Figs. 2 and 3, these curves also suggest that large percentage differences, which occur at small PIF values, lead to poorer performance by the maximum likelihood location estimator, and that small

Table 2. Performance of the PIF = 0 and PIF = 13 maximum likelihood location estimators for $100\times$ 2D Gaussian PSF data sets simulated using PIF = 13 under scenarios 1 and 2 of Table 1, with the Gaussian width σ_g as shown and all other parameters as given in Section 3.1. For each data set, the difference $d(x_0)$ between the median of the x_0 estimates and the true value x_0, and the percentage difference $\delta(x_0)$ between the standard deviation (with respect to the median) of the x_0 estimates and the limit of the x-localization accuracy, for both the PIF = 0 and PIF = 13 estimators, are shown.

σ_g (nm)	Scenario 1				Scenario 2			
	$d(x_0)$ (nm)		$\delta(x_0)$ (%)		$d(x_0)$ (nm)		$\delta(x_0)$ (%)	
	PIF 13	PIF 0	PIF 13	PIF 0	PIF 13	PIF 0	PIF 13	PIF 0
72.94	0.04	-5.85	1.34	2.58	-0.11	-11.42	1.50	-3.83
78.56	-0.10	-3.76	-0.75	1.47	-0.10	-7.42	3.65	6.09
85.10	0.01	-1.88	-4.00	-2.40	-0.01	-3.73	2.02	6.19
92.84	-0.11	-0.89	-3.35	-2.50	-0.01	-1.26	0.36	2.93
102.12	-0.02	-0.24	0.98	1.26	0.17	0.11	2.42	2.52
113.47	0.02	-0.02	-2.66	-2.57	0.19	0.38	-0.87	-0.49

percentage differences, which occur at large PIF values, lead to better performance by the estimator. To obtain a conservative guideline for determining the minimum PIF value, we specify the stringent requirement that a given PIF is appropriate only if its corresponding PSF is no more than 1% different from the benchmark PSF. Applying this guideline, we see a difference between the curves for the two magnifications. For the $63\times$ magnification, a minimum PIF value of 9 is required for both the Airy PSF and the 2D Gaussian PSF. For the $100\times$ magnification, the minimum PIF value is 7 for both PSFs. This difference between the magnifications corroborates the above finding that the performance of the maximum likelihood estimator at higher magnifications is impacted to a lesser extent by the use of smaller PIF values.

The minimum PIF values based on the 1% guideline appear to be reasonable. For the $63\times$ magnification, the minimum PIF value of 9 approximately coincides with the point at which the difference d and the percentage difference δ begin to level off in the plots of Figs. 2 and 3. The same is observed for the minimum PIF value of 7 for the $100\times$ magnification, and in some cases it lies within the part of the curve that is already essentially level with the value at PIF = 13.

4. STUDY 2: MICROSPHERE LOCALIZATION BY PSF FITTING

Despite the fact that the image of a small microsphere is indeed comparable to the PSF, there is nevertheless a mismatch between them. The mismatch naturally becomes even more significant when larger microspheres are considered. In light of this, the goal of our study is to determine whether the fitting of a PSF to the image of a microsphere is a suitable method of microsphere localization. We specifically investigate the maximum likelihood fitting of an Airy PSF to simulated microsphere image data, and based on the performance of the estimator, present findings that are dependent on the size of the microsphere. Two approaches to the localization are considered, one in which the width of the Airy PSF is fixed, and one in which it is floated and estimated simultaneously with the positional coordinates.

4.1 Method of investigation

As we are particularly interested in the impact of microsphere size on the suitability of PSF fitting for microsphere localization, we carry out estimations on simulated images of microspheres ranging from a small diameter of 50 nm to a relatively large diameter of 1 μm. Each data set consists of 1000 repeat CCD images of an in-focus microsphere which were simulated as described in Section 2.2 using the image function of Eq. (4), and was subjected to maximum likelihood localization that fits an Airy PSF (Eq. (2)) to the data.

To account for microspheres of different colors, data sets were simulated with the wavelength of the detected photons set to $\lambda = 485$ nm, $\lambda = 573$ nm, and $\lambda = 663$ nm. For all data sets, the image size is 17×17 pixels, and the pixel size is 14 μm $\times$ 14 μm. The microsphere is positioned such that its image is centered at 8.3 pixels in the x direction and 8.1 pixels in the y direction within the 17×17-pixel image. Given a magnification of
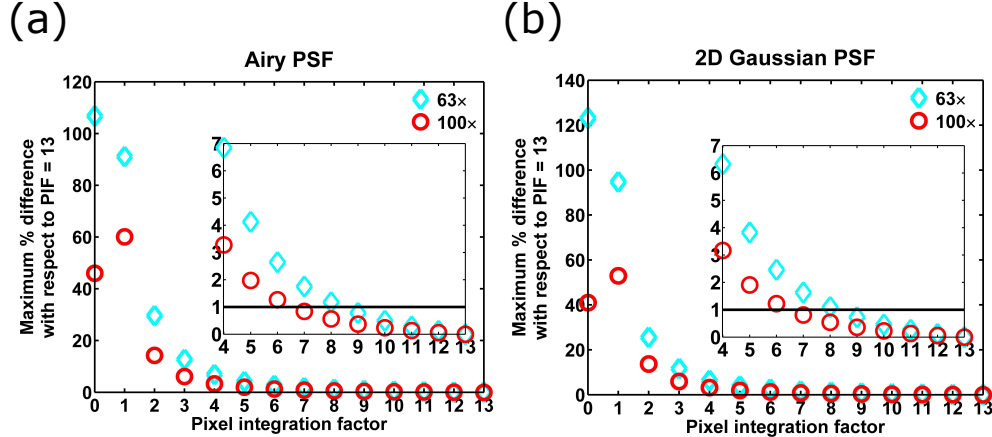
Figure 5. Obtaining a guideline for the selection of a suitable fineness of PSF integration. The maximum percentage difference, as described in Section 3.3, between the PSF computed using a given PIF value and the benchmark PSF computed using PIF = 13, is shown as a function of the PIF value for the former for (a) the Airy PSF and (b) the 2D Gaussian PSF. In both (a) and (b), the PSFs are computed using the relevant parameters given in Section 3.1, and the maximum percentage difference is shown for both the 63× (cyan ◇) and the 100× (red ○) magnifications. The inset shows the maximum percentage difference for PIF values ranging from 4 to 13, with the horizontal line marking 1%.

$M = 100$, this corresponds to positional coordinates $\theta = (x_0, y_0) = (1162 \text{ nm}, 1134 \text{ nm})$ for the microsphere, as the origin of the coordinate system is taken to be the upper left corner of the 17×17-pixel image. Also for all data sets, we assume the use of an oil immersion objective lens with numerical aperture $n_a = 1.4$, and the use of an immersion oil of refractive index $n = 1.518$. These values, along with the wavelength for the particular data set, were used in the computation of the Born and Wolf PSF of Eq. (5). Furthermore, the average number of photons detected from the microsphere per image is $N_{photon} = 2000$, the average number of background photons per pixel is $\beta_0 = 90$, and the mean and standard deviation of the readout noise in each pixel are $\eta_0 = 0$ electrons and $\sigma_0 = 6$ electrons, respectively.

The data sets considered here differ from those analyzed in our previous report[23] primarily by the 140-nm effective pixel size of the microsphere images. In the previous work, effective pixel sizes of ∼205 nm and 160 nm were considered.

For a given data set, the width parameter α of the fitted Airy PSF is set to its theoretical value of $2\pi n_a/\lambda$ in the estimation approach that fixes the width of the PSF. In the approach that floats the width, α is estimated along with the positional coordinates, so that the vector of parameters to be estimated is given by $\theta = (x_0, y_0, \alpha)$.

4.2 Quantifying and evaluating estimator performance

For a given data set, the performance of the maximum likelihood estimator is quantified the same way as in the fineness of PSF integration study, except that the mean, instead of the median, of the estimates is used to compute the difference of Eq. (11) and the percentage difference of Eq. (12) for each positional coordinate.

The estimator's performance is deemed satisfactory, and hence the localization of the microsphere by the fitting of an Airy PSF is considered suitable, if, for each positional coordinate, the distance between the mean of the estimates and the true value is within three times the standard error of the mean, and the distance between the variance of the estimates and the square of the limit of the localization accuracy is within three times the standard error of the variance. (Note that the distance refers to the magnitude of the difference between the two quantities.) So that the performance of the estimator is evaluated against the best performance possible, the standard errors are defined based on the performance of an ideal estimator. Specifically, the standard error of the mean, for a given positional coordinate, is defined as

$$SE_{mean} = \frac{\sigma_{ideal}}{\sqrt{N_{sample}}} = \frac{\delta}{\sqrt{N_{sample}}}, \tag{13}$$

where σ_{ideal} is the standard deviation, in the ideal case, of an unbiased estimator that attains the limit of the localization accuracy δ for the positional coordinate. Since the data here consists of simulated CCD images of microspheres, the limit of accuracy δ is calculated using the Fisher information expression of Eq. (9), with the underlying image function given by Eq. (4). The quantity N_{sample} is the sample size, given by the number of estimates from which the mean and standard deviation of the estimates are calculated for the data set. For most data sets presented in this paper, no estimates are discarded, and N_{sample} is just the number of images comprising the data set. For a few data sets, a small fraction (<5% for the majority of cases) of the pairs of x_0 and y_0 estimates are discarded for placing the microsphere outside the pixel array comprising its image, in which case N_{sample} is the number of pairs of x_0 and y_0 estimates that are retained.

Note that whereas δ is used in this study to denote the limit of accuracy, it is used to denote the percentage difference between the standard deviation of the estimates and the limit of accuracy in the fineness of PSF integration study (see Eq. (12)). We have chosen to maintain this notational discrepancy so that the presentation of the two independent studies here is kept consistent with the presentation of their respective previous reports.[22, 23]

The standard error of the variance, using the same notation as in Eq. (13), is given by

$$SE_{var} = \sigma_{ideal}^2 \cdot \sqrt{\frac{2}{N_{sample} - 1}} = \delta^2 \cdot \sqrt{\frac{2}{N_{sample} - 1}}. \tag{14}$$

This expression is predicated on the distribution of estimates in the ideal case being Gaussian. This is a justifiable assumption, since in the absence of a mismatch between the data and the fitted model, the maximum likelihood estimator, which is known to be asymptotically Gaussian distributed with variance given by the Cramér-Rao lower bound, has been observed to produce x_0 and y_0 estimates whose histograms are well fitted by a Gaussian curve with mean and standard deviation given by those of the estimates. This is the case for the results presented in Section 4.3 involving data sets that were simulated and fitted using the microsphere image model of Eq. (4).

For both the mean and the variance, we choose the criterion to be three times their respective standard errors based on the idea that the performance of the estimator should be comparable to its performance in the absence of a mismatch between the data and the fitted model. As shown in Table 3, when maximum likelihood estimation that fits an Airy PSF, with and without the simultaneous estimation of the width of the Airy PSF, is used to localize a molecule whose image is simulated with the Airy PSF itself using the applicable parameters given in Section 4.1 for a microsphere image, the resulting distances that quantify the estimator's performance mostly fall within two times, but can occasionally fall between two and three times, the respective standard errors for an ideal estimator. (For the analysis of these data sets, the limit of accuracy δ is calculated using the Fisher information expression of Eq. (9), with the underlying image function given by Eq. (2). Also, for the case where the width of the Airy PSF is estimated, δ is calculated with $\theta = (x_0, y_0, \alpha)$.) Note that even though for all cases in Table 3 the distance between the mean of the estimates and the true value is within two times the standard error of the mean, it was observed, for analogous data sets analyzed previously,[23] to occasionally fall between two and three times the standard error of the mean. Based on these findings, as well as results[12] suggesting that a mismatch between the data and the fitted model can lead to a significant difference between the standard deviation of the estimates and the limit of accuracy, we arrive at three times the standard error as the criterion for the fitting of an Airy PSF to microsphere images. To give a more informative view of our results, however, we highlight the cases where the more stringent criterion of two times the standard error is satisfied.

4.3 Results and Discussion

For each of the three wavelengths $\lambda = 485$ nm, $\lambda = 573$ nm, and $\lambda = 663$ nm, we plot, as a function of microsphere size, the difference between the mean of the x_0 estimates and the true value x_0, and the difference between the mean of the y_0 estimates and the true value y_0. For a given microsphere size, the differences are highlighted in green if both of their magnitudes are within the criterion of three times their respective standard errors of the mean, and in red if both of their magnitudes are within two times their respective standard errors of the mean. In a separate plot, we also show, as a function of microsphere size, the percentage difference between the x-localization accuracy (i.e., the standard deviation of the x_0 estimates) and the limit of the x-localization accuracy, and the percentage difference between the y-localization accuracy (i.e., the standard deviation of the

Table 3. Maximum likelihood point source localization. Results are shown for three data sets, each corresponding to a different wavelength λ, and each consisting of 1000 repeat images of a point source simulated with an Airy PSF, using the applicable parameters specified in Section 4.1. For each data set, estimation is carried out with a fixed width Airy PSF and a floated width Airy PSF. In the latter case, the width parameter α of the Airy PSF is estimated along with its positional coordinates x_0 and y_0. For each data set, the mean and accuracy (i.e., standard deviation SD) of the x_0 and y_0 estimates are shown alongside their respective true values and accuracy limits δ. For each coordinate, superscript $*$ for the difference (mean − true) indicates |mean − true| is within 2 times the standard error of the mean SE_{mean} (Eq. (13)) for an ideal estimator. Superscripts † and $*$ for the % difference between SD and δ indicate $|SD^2 - \delta^2|$ is between 2 and 3 times, and within 2 times, the standard error of the variance SE_{var} (Eq. (14)) for an ideal estimator, respectively.

	λ (nm)		True value (nm)	Mean of estimates (nm)	Mean − True (nm)	δ (nm)	SD (nm)	$(SD - \delta)/\delta$ $\times 100$ (%)
Fixed width	485	x_0	1162.00	1161.99	-0.01^*	2.74	2.69	-1.75^*
		y_0	1134.00	1134.01	0.01^*	2.78	2.87	3.44^*
	573	x_0	1162.00	1161.99	-0.01^*	3.23	3.19	-1.15^*
		y_0	1134.00	1134.03	0.03^*	3.39	3.34	-1.27^*
	663	x_0	1162.00	1161.86	-0.14^*	3.87	3.82	-1.27^*
		y_0	1134.00	1133.88	-0.12^*	3.94	3.72	$-5.66^\dagger$
Floated width	485	x_0	1162.00	1161.91	-0.09^*	2.80	2.72	-2.70^*
		y_0	1134.00	1133.99	-0.01^*	2.79	2.91	4.19^*
	573	x_0	1162.00	1161.97	-0.03^*	3.23	3.20	-1.13^*
		y_0	1134.00	1134.01	0.01^*	3.39	3.34	-1.29^*
	663	x_0	1162.00	1161.86	-0.14^*	3.88	3.83	-1.38^*
		y_0	1134.00	1133.89	-0.11^*	3.94	3.72	$-5.60^\dagger$

y_0 estimates) and the limit of the y-localization accuracy. The percentage difference is color-coded as in the case of the difference between the mean and the true value, but based instead on the comparison of the standard error of the variance with the magnitude of the difference between the square of the localization accuracy (i.e., the variance of the estimates) and the square of the limit of the localization accuracy.

When the width of the fitted Airy PSF is fixed to its theoretical value during the maximum likelihood localization, the plots in Fig. 6 show that, for both the mean and the standard deviation of the location estimates, the criterion of three times the standard error is satisfied for both the x_0 and y_0 coordinates only up to a certain microsphere size. This is in agreement with the idea that since a microsphere is the most point-like when it is small, localization by fitting with an Airy PSF should only be suitable for the localization of the smallest microspheres. The precise cutoff diameter depends, in our current case, on the color of the microsphere. For example, taking the smallest size that satisfies both standard error-based criteria, the plots for $\lambda = 485$ nm and $\lambda = 663$ nm suggest that microspheres up to 100 nm in diameter can be localized with acceptable performance using an Airy PSF. However, the plots for $\lambda = 573$ nm suggest that the cutoff should be smaller at 50 nm. On the whole, based on the results for the three wavelengths shown in Fig. 6, as well as comparable results, not shown here, from the analysis of a second set of statistically identical data sets, we find 100 nm to be a reasonable and generally applicable rule-of-thumb cutoff diameter for localization using a fixed width Airy PSF.

When the width of the fitted Airy PSF is floated and estimated along with the positional coordinates during the maximum likelihhood localization, the plots in Fig. 7 show that, for both the mean and the standard deviation of the location estimates, the criterion of three times the standard error is satisfied for both the x_0 and y_0 coordinates for essentially all the microsphere sizes considered. This is in sharp contrast with the results of Fig. 6, but is not surprising because by being able to adjust the width of the fitted Airy PSF to better match the PSF to the image of a larger microsphere, the estimator is expected to be capable of localizing larger microspheres with acceptable performance. Based on the results shown in Fig. 7, and similar results, not shown here, from the analysis of a second set of statistically identical data sets, we find that the fitting of a floated width Airy PSF enables the localization of microspheres as large as, or at least nearly as large as, 1 μm in diameter.
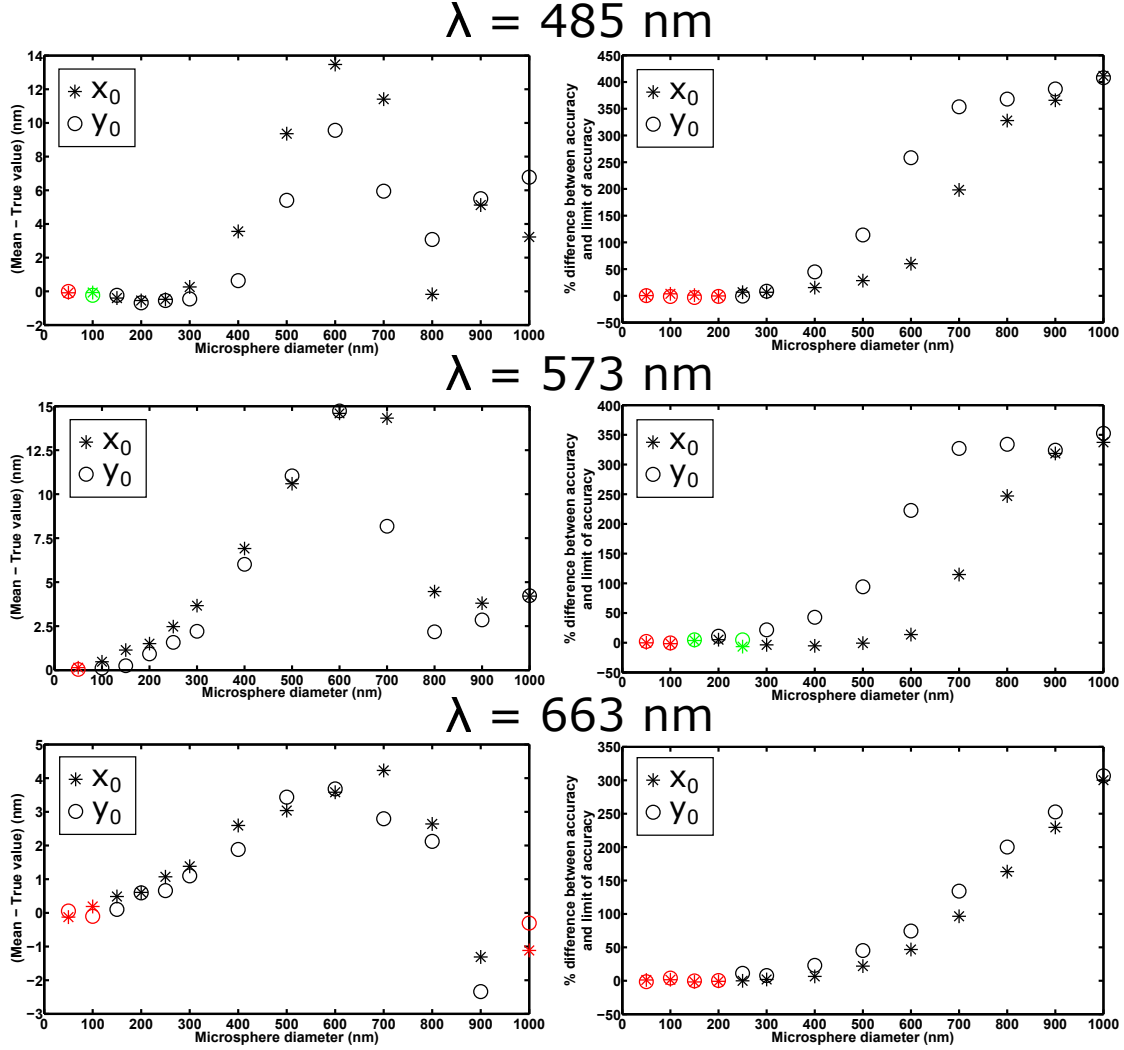
Figure 6. Analysis of the mean and accuracy (i.e., standard deviation) of estimates from the maximum likelihood localization of microspheres with a fixed width Airy PSF. For each of three detection wavelengths λ, the mean and accuracy of the estimates for 13 data sets are analyzed in two separate plots. Each data set comprises 1000 repeat images of a microsphere of a different size, simulated with the parameters given in Section 4.1. In the analysis of the mean for each data set, the differences between the mean of the x_0 estimates and the true value x_0, and between the mean of the y_0 estimates and the true value y_0, are plotted in green and red if both of their magnitudes are within 3 and 2 times, respectively, their respective standard errors of the mean (Eq. (13)) for an ideal estimator. Similarly, in the analysis of the accuracy for each data set, the percentage differences between the x-localization accuracy and the limit of the x-localization accuracy, and between the y-localization accuracy and the limit of the y-localization accuracy, are plotted in green and red if the corresponding absolute differences between the square of the localization accuracy (i.e., the variance of the estimates) and the square of the limit of accuracy are both within 3 and 2 times, respectively, their respective standard errors of the variance (Eq. (14)) for an ideal estimator.

Note that there are unexpected exceptions to this general rule, however, most notably in the failure of the estimator, in the case of $\lambda = 485$ nm, to satisfy the standard error of the mean criterion for the relatively small diameters of 100 nm, 150 nm, and 200 nm. These exceptions are reproduced in the analysis of the second set of statistically identical data sets, and are at least partially attributable to the relatively coarse 140-nm effective pixel size of the microsphere image data. By increasing the magnification to $M = 150$, thereby reducing the effective pixel size to ~93 nm, for example, the maximum likelihood estimator is able to satisfy the standard
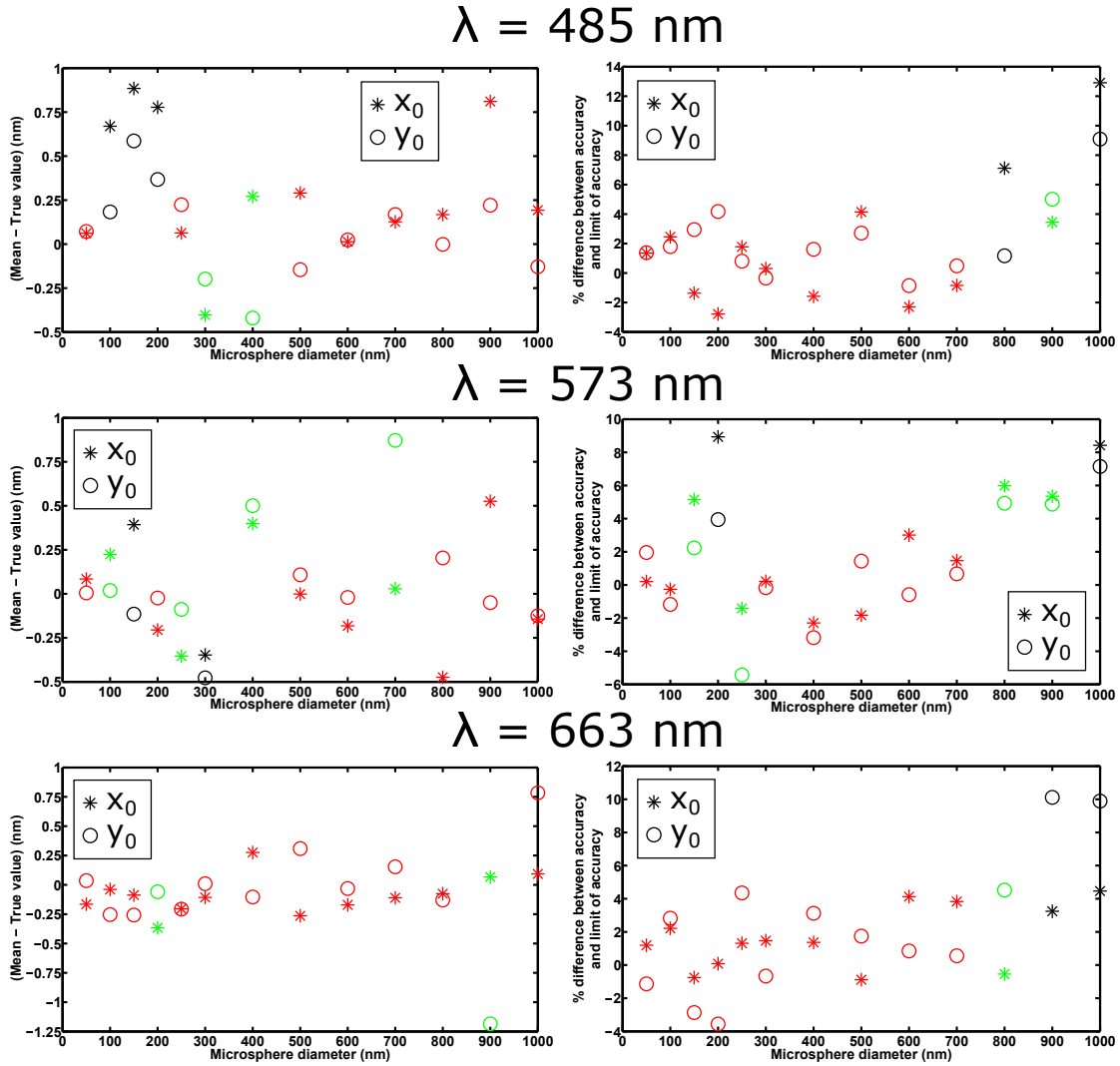
Figure 7. Analysis of the mean and accuracy (i.e., standard deviation) of estimates from the maximum likelihood localization of microspheres with a floated width Airy PSF. The results shown are obtained from localization carried out on the same data sets as in Fig. 6, but with the width parameter α of the fitted Airy PSF estimated along with its positional coordinates x_0 and y_0. All details are as given in Fig. 6.

error of the mean criterion for each of these three small diameters. This can be seen in Fig. 8, where the results from the fitting of a fixed width Airy PSF are also shown. These results, too, are corroborated by those obtained from the analysis of a second set of statistically identical data sets.

Note also that image pixelation plays a role here because of the mismatch between the microsphere data and the fitted Airy PSF. We show in Table 4 that by fitting the microsphere image model itself instead of an Airy PSF to the three data sets with the relatively coarse 140-nm effective pixel size, the standard error of the mean criterion is satisfied.

ACKNOWLEDGMENTS
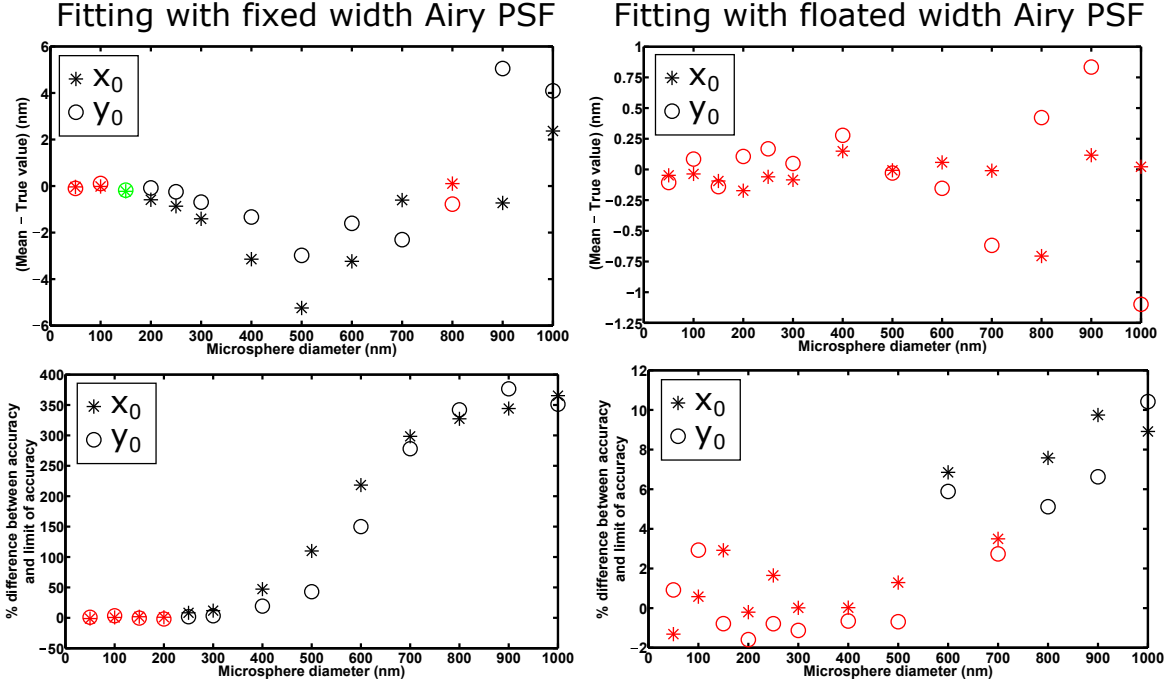
Figure 8. Analysis of the mean and accuracy (i.e., standard deviation) of estimates from the maximum likelihood localization of microspheres with a fixed width (left-hand side plots) and a floated width (right-hand side plots) Airy PSF. Results are shown for 13 data sets, each consisting of 1000 repeat images of a microsphere of a different size, simulated with wavelength $\lambda = 485$ nm and the parameters given in Section 4.1, except the magnification has been changed to $M = 150$ to yield a smaller effective pixel size of approximately 93 nm, the image and the per-pixel mean background photon count have accordingly been changed to a 23×23-pixel array and $\beta_0 = 40$, respectively, to retain the detection of similar numbers of photons from the microsphere and the background component, and the lateral location of the microsphere has been changed to 11.3 pixels in the x direction and 11.1 pixels in the y direction within the 23×23-pixel array. For each data set, the difference between the mean of the estimates and the true value for each positional coordinate, and the percentage difference between the localization accuracy and the limit of the localization accuracy for each positional coordinate, are color-coded as in Figs. 6 and 7.

Table 4. Maximum likelihood microsphere localization with the microsphere image model. Results are shown for localization carried out on the first 500 images of the 100-nm, 150-nm, and 200-nm data sets, for the detection wavelength $\lambda = 485$ nm, from Figs. 6 and 7. Each image in a data set was fitted with the microsphere image model used to generate the data set, and only the positional coordinates x_0 and y_0 were estimated. For each data set, the mean and accuracy (i.e., standard deviation SD) of the x_0 and y_0 estimates are shown alongside their respective true values and accuracy limits δ. For each coordinate, superscript $*$ for the difference (mean − true) indicates |mean − true| is within 2 times the standard error of the mean SE_{mean} (Eq. (13)) for an ideal estimator. Similarly, superscript $*$ for the % difference between SD and δ indicates |SD$^2 - \delta^2$| is within 2 times the standard error of the variance SE_{var} (Eq. (14)) for an ideal estimator. Absence of the superscript indicates |SD$^2 - \delta^2$| is greater than 3 times SE_{var}.

d (nm)		True value (nm)	Mean of estimates (nm)	Mean − True (nm)	δ (nm)	SD (nm)	$(SD - \delta)/\delta$ ×100 (%)
100	x_0	1162.00	1161.99	−0.01*	2.93	3.20	9.15
	y_0	1134.00	1133.90	−0.10*	2.99	3.08	2.91*
150	x_0	1162.00	1162.07	0.07*	3.14	3.16	0.60*
	y_0	1134.00	1134.01	0.01*	3.21	3.08	−4.26*
200	x_0	1162.00	1162.03	0.03*	3.44	3.35	−2.60*
	y_0	1134.00	1133.85	−0.15*	3.52	3.50	−0.48*

REFERENCES

[1] Betzig, E., Patterson, G. H., Sougrat, R., Lindwasser, O. W., Olenych, S., Bonifacino, J. S., Davidson, M. W., Lippincott-Schwartz, J. and Hess, H. F., "Imaging intracellular fluorescent proteins at nanometer resolution," *Science* **313**(5793), 1642–1645 (2006).

[2] Rust, M. J., Bates, M. and Zhuang, X., "Sub-diffraction-limit imaging by stochastic optical reconstruction microscopy (STORM)," *Nat. Methods* **3**(10), 793–795 (2006).

[3] Hess, S. T., Girirajan, T. P. K. and Mason, M. D., "Ultra-high resolution imaging by fluorescence photoactivation localization microscopy," *Biophys. J.* **91**(11), 4258–4272 (2006).

[4] Ram, S., Prabhat, P., Ward, E. S. and Ober, R. J., "Improved single particle localization accuracy with dual objective multifocal plane microscopy," *Opt. Express* **17**(8), 6881–6898 (2009).

[5] Metcalf, D. J., Edwards, R., Kumarswami, N. and Knight, A. E., "Test samples for optimizing STORM super-resolution microscopy," *J. Vis. Exp.* (79), e50579 (2013).

[6] Zessin, P. J. M., Krüger, C. L., Malkusch, S., Endesfelder, U. and Heilemann, M., "A hydrophilic gel matrix for single-molecule super-resolution microscopy," *Opt. Nanoscopy* **2**, 4 (2013).

[7] Churchman, L. S., Ökten, Z., Rock, R. S., Dawson, J. F. and Spudich, J. A., "Single molecule high-resolution colocalization of Cy3 and Cy5 attached to macromolecules measures intramolecular distances through time," *Proc. Natl. Acad. Sci. USA* **102**(5), 1419–1423 (2005).

[8] Malkusch, S., Endesfelder, U., Mondry, J., Gelléri, M., Verveer, P. J. and Heilemann, M., "Coordinate-based colocalization analysis of single-molecule localization microscopy data," *Histochem. Cell Biol.* **137**(1), 1–10 (2012).

[9] Erdelyi, M., Rees, E., Metcalf, D., Kaminski Schierle, G. S., Dudas, L., Sinko, J., Knight, A. E. and Kaminski, C. F., "Correcting chromatic offset in multicolor super-resolution localization microscopy," *Opt. Express* **21**(9), 10978–10988 (2013).

[10] Ober, R. J., Ram, S. and Ward, E. S., "Localization accuracy in single-molecule microscopy," *Biophys. J.* **86**(2), 1185–1200 (2004).

[11] Smith, C. S., Joseph, N., Rieger, B. and Lidke, K. A., "Fast, single-molecule localization that achieves theoretically minimum uncertainty," *Nat. Methods* **7**(5), 373–375 (2010).

[12] Abraham, A. V., Ram, S., Chao, J., Ward, E. S. and Ober, R. J., "Quantitative study of single molecule location estimation techniques," *Opt. Express* **17**(26), 23352–23373 (2009).

[13] Sergé, A., Bertaux, N., Rigneault, H. and Marguet, D., "Dynamic multiple-target tracing to probe spatiotemporal cartography of cell membranes," *Nat. Methods* **5**(8), 687–694 (2008).

[14] Born, M. and Wolf, E., [*Principles of Optics*], Cambridge University Press, Cambridge, UK (1999).

[15] Kubitscheck, U., Kückmann, O., Kues, T. and Peters, R., "Imaging and tracking of single GFP molecules in solution," *Biophys. J.* **78**(4), 2170–2179 (2000).

[16] Cheezum, M. K., Walker, W. F. and Guilford, W. H., "Quantitative comparison of algorithms for tracking single fluorescent particles," *Biophys. J.* **81**(4), 2378–2388 (2001).

[17] Thompson, R. E., Larson, D. R. and Webb, W. W., "Precise nanometer localization analysis for individual fluorescent probes," *Biophys. J.* **82**(5), 2775–2783 (2002).

[18] Gibson, S. F. and Lanni, F., "Experimental test of an analytical model of aberration in an oil-immersion objective lens used in three-dimensional light microscopy," *J. Opt. Soc. Am. A* **8**(10), 1601–1613 (1991).

[19] Preza, C., Ollinger, J. M., McNally, J. G. and Thomas, L. J. Jr., "Point-spread sensitivity analysis for computational optical-sectioning microscopy," *Micron Microsc. Acta* **23**(4), 501–513 (1992).

[20] Cole, R. W., Jinadasa, T. and Brown, C. M., "Measuring and interpreting point spread functions to determine confocal microscope resolution and ensure quality control," *Nat. Protoc.* **6**(12), 1929–1941 (2011).

[21] Rao, C. R., [*Linear Statistical Inference and Its Applications*], Wiley, New York, USA (1965).

[22] Chao, J., Ram, S., Lee, T., Ward, E. S. and Ober, R. J., "Investigation of the numerics of point spread function integration in single molecule localization," *Opt. Express* **23**(13), 16866–16883 (2015).

[23] Chao, J., Lee, T., Ward, E. S. and Ober, R. J., "Fluorescent microspheres as point sources: a localization study," *PLoS ONE* **10**(7), e0134112 (2015).

[24] Ram, S., Ward, E. S. and Ober, R. J., "A stochastic analysis of performance limits for optical microscopes," *Multidim. Syst. Sign. P.* **17**(1), 27–57 (2006).